JOURNAL OF SOLID STATE CHEMISTRY 103, 105–113 (1993)

Refinement of the Structures of the Layer Silicates MCuSi$_4$O$_{10}$ (M = Ca, Sr, Ba) by Rietveld Analysis of Neutron Powder Diffraction Data

BRYAN C. CHAKOUMAKOS, JAIME A. FERNANDEZ-BACA, AND LYNN A. BOATNER

Solid State Division, Oak Ridge National Laboratory, Oak Ridge, Tennessee 37831-6056

Received April 22, 1992; in revised form August 6, 1992; accepted August 10, 1992

The MCuSi$_4$O$_{10}$ (M = Ca, Sr, Ba) compounds possess the gillespite (BaFeSi$_4$O$_{10}$) structure, which is tetragonal, $P4/ncc$, Z = 4. Data sets of 2365 step intensities were recorded for the title compounds with λ = 1.400 Å at T = 295 K. For M = Ca, a = 7.3017 (3) Å, c = 15.1303 (6) Å, V_{cell} = 806.66 (9) Å^3, R_{exp} = 0.0453, R_{wp} = 0.0515, for 487 reflections. For M = Sr, a = 7.3707 (2) Å, c = 15.5904 (6) Å, V_{cell} = 846.9 (1) Å^3, R_{exp} = 0.0433, R_{wp} = 0.0489, for 521 reflections. For M = Ba, a = 7.4409 (3) Å, c = 16.1367 (8) Å, V_{cell} = 893.4 (1) Å^3, R_{exp} = 0.0466, R_{wp} = 0.0522, for 546 reflections. The gillespite structure contains an unbranched single silicate layer, which can be viewed as a tesselation of corner-linked Si$_4$O$_{10}$ rings. The Cu in MCuSi$_4$O$_{10}$ is in square-planar coordination with the nonbridging oxygens of the corrugations of the silicate layer. The alkaline-earth atom, in distorted cubic coordination, joins together adjacent [CuSi$_4$O$_{10}$]$^{2-}$ slabs. Increasing the size of the alkaline-earth atom increases the cell dimensions anisotropically (i.e., $\Delta c > \Delta a$) due to the inflexibility of the silicate anion. Room-pressure experiments show no evidence for oxygen intercalation or polytypism. The lattice mismatch between the [CuSi$_4$O$_{10}$]$^{2-}$ slabs of the gillespite structure type and the square-planar CuO$_2$ layers of the superconducting cuprates is small, which suggests possible applications of these materials as exotic thin-film substrates for the high T_c cuprates or other novel structures having cuprate and silicate layers.

Introduction

The structure of gillespite (BaFeSi$_4$O$_{10}$) was determined initially by Pabst (*1*) using film methods and it has subsequently been refined in the course of extended X-ray diffraction studies of its high-pressure phase transition (*2–4*). That the compounds MCuSi$_4$O$_{10}$ (M = Ca, Sr, Ba) are isostructural with gillespite was also confirmed by Pabst (*5*), who made an early refinement of the M = Ca structure by film methods. The compounds MCuSi$_4$O$_{10}$ (M = Ca, Sr, Ba) are an intense blue color, and the Ca analog ("Egyptian blue") has been used as a pigment since ancient times [see the history given in Pabst (*5*)].

The gillespite structure contains an unbranched single silicate layer, $\{\mathbf{uB},1^2_\infty\}$ [^{4}Si$_4$O$_{10}$] (*6*). This silicate anion can be viewed as a tesselation of corner-linked Si$_4$O$_{10}$ rings, each with C_{4v} point symmetry. The Cu in MCuSi$_4$O$_{10}$ is in square-planar coordination with the nonbridging oxygens, and is nestled in the corrugations of the silicate layer. The alkaline-earth atom, in distorted cubic coordination, joins together adjacent [CuSi$_4$O$_{10}$]$^{2-}$ slabs. The structure has

0022-4596/93 $5.00

an 8-Å subcell parallel to c, but alternate left- and right-handed rotations of four-membered silicate tetrahedral rings cause the c dimension to be doubled to 16 Å (*1*, *3*). Gillespite undergoes a reversible first-order phase transition at 18 kbar (*2*); the volume discontinuity at the gillespite I → II transition is a consequence of increased coordination of the barium and iron. The high-pressure form, gillespite II (orthorhombic, $P2_12_12$), differs from the room-pressure phase in that all four-membered rings in adjacent silicate layers have the same rotational sense (viewed along c). The existence of several different layer orientations in gillespite I and II allows the possible occurrence of several stacking polytypes and twinning mechanisms, which have been enumerated by Hazen (*7*).

In the present work, the title compounds have been refined by Rietveld analysis of neutron powder diffraction data to: (1) explore the possibility of polytypism in compounds isostructural with gillespite; (2) provide modern structure refinements; (3) examine the lattice mismatch with (Ca,Sr) CuO_2 layers of the superconducting cuprates for the purpose of designing novel layered cuprates and exotic superconducting thin-film substrates; and (4) to explore the structural systematics (i.e., possible oxygen intercalation, bond length and angle variations, comparisons with gillespite, possible high-pressure polymorphism).

Experimental

Single crystals (up to $1 \times 0.5 \times 0.5$ mm^3) of $BaCuSi_4O_{10}$ are often grown incidently, during the crystal growth of $YBa_2Cu_3O_{7-d}$ and are formed as a reaction between silicon carbide ceramic, furnace hearth-plates and overflowing Ba–Cu–O melts. For the purposes of this study and subsequent high-pressure studies, powder samples of the title compounds were prepared by solid-state reaction of high-purity SiO_2 (α-quartz), CuO, $CaCO_3$, $SrCO_3$, and $BaCO_3$ at 1323 K in flowing oxygen. The oxide mixtures were reacted as loose powders in Pt crucibles. To achieve phase purity, the samples were fired, reground, and sieved (100 mesh or 150 microns) several times at increasing temperatures from 1073 K (initial) to 1323 K (final) or 1353 K (final) for the Ba analog. One of the early grindings was made for 10 minutes duration with a McCrone micronizing mill using a methanol slurry. The SiO_2 in the form of α-quartz reacts sluggishly; residual amounts are converted to tridymite before complete reaction is achieved. At each firing temperature, the samples sintered although little grain growth occurred. Phase purity was monitored by powder X-ray diffraction (XRD) and judged to be complete by comparison with the powder diffraction file (PDF) reference patterns. Trace impurities, below 2 volume%, may not be detectable by this method. The perfect {001} cleavage in these compounds should produce preferred orientation in the sample mounts, however, very little could be detected by XRD for the finely ground samples. All three compounds have an intense blue color, but the color changed reversibly from a lighter to a darker shade depending upon whether the final firing was in oxygen or air, respectively. This observation suggests the possibility of oxygen intercalation.

The neutron diffraction data were collected on the HB-4 high-resolution powder diffractometer at the High Flux Isotope Reactor at ORNL. This instrument has a Ge (115) monochromator which, when $2\theta = 80°$, selects an incident neutron beam of $\lambda \approx 1.4$ Å. The neutron wavelength was determined more precisely to be 1.3996 Å on the basis of unit cell refinements for a nickel powder standard. Soller slit collimators of 12′ and 20′ are positioned before and after the monochromator crystal, respectively. An array of 32 equally spaced (2.7°) ^{3}He detectors, each with a 6′ mylar foil collimator, can be step-scanned over a range up

to 40° for scattering angles between 11° and 135° 2θ. The samples were placed in rotating (15 rpm) vanadium cans (9 mm I.D. × 6 cm) for data collection at 295 K over the 2θ range of 11° to 135° in steps of 0.05°. For each step, diffracted beams were accumulated for 90 sec. For these data collections, the detector array scanned the largest 2θ range allowable, i.e., ~40°, which has the effect of overlapping up to 15 detectors for steps in the middle of the pattern. Overlapping detectors for a given step serves to average the counting efficiency and the 2θ zero-point shift for each detector.

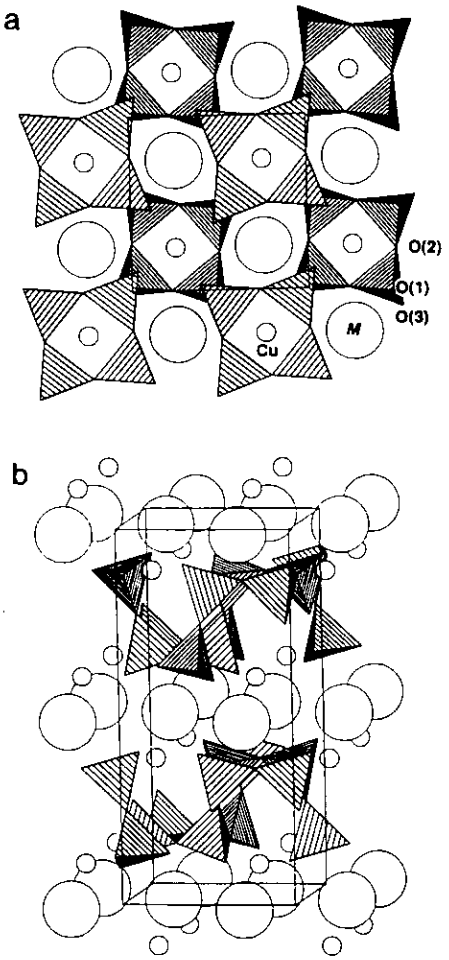

FIG. 1. STRUPLO projections (2θ) of: (a) one-half of the cell (outlined) thickness viewed along [001] and (b) axiometric view with c vertical. The shaded tetrahedra represent SiO_4 units, the large circles, alkaline-earth ions, and the small circles, Cu atoms.

TABLE I

CRYSTAL DATA FOR MCuSi$_4$O$_{10}$ (M = Ca, Sr, Ba) STRUCTURE REFINEMENTS

	CaCuSi$_4$O$_{10}$	SrCuSi$_4$O$_{10}$	BaCuSi$_4$O$_{10}$
R_{wp}	0.0515	0.0489	0.0522
R_p	0.0448	0.0427	0.0456
R_{exp}	0.0453	0.0433	0.0466
G-of-F	1.29	1.27	1.25
a(Å)	7.3017 (3)	7.3707 (2)	7.4409 (3)
c(Å)	15.1303 (6)	15.5904 (6)	16.1367 (8)
V (Å^3)	806.66 (9)	846.9 (1)	893.4 (1)
M_r	375.96	423.50	473.21
D_x (g/cm^3)	3.095	3.320	3.517
Reflections	487	521	546
μR			
Preferred orientation, R_0[a]	1.022 (3)	1.019 (4)	1.008 (4)

[a] For this diffraction geometry and platy crystallite shape, the refined coefficient, R_0, gives the effective sample compression ($R_0 > 1$) along the cylinder axis. If no preferred orientation exists, $R_0 = 1$.

The least-squares structure refinements were made with the computer program package GSAS (*8*), which uses a full-profile Rietveld analysis (*9*). Previous refinements of monoclinic ZrO_2 (IUCr Rietveld round-robin sample) showed a significantly improved fit using the pseudo-Voigt peak-profile function (described by Thompson *et al.* (*10*)) as compared to the Voigt peak-profile function (*9*), without marked changes in the refined structural parameters, but with smaller standard errors. This implies that data from the HB-4 diffractometer is relatively high resolution, and the use of the pseudo-Voigt peak-profile function is appropriate. In the GSAS software, the pseudo-Voigt function is integrated using a multi-term Simpson's rule (*11*). A detailed description of the peak-profile function parameters and their interpretation is given by Larson and Von Dreele (*8*) and Von Dreele (*12*); the essential features are summarized here. The 2θ difference, ΔT, is modified for asymmetry, A_S, and sample

shift, S_S, as $\Delta T' = \Delta T + f_i A_S/\tan 2\theta + S_S \cos\theta$. The width of the peak, σ^2, varies with 2θ as $\sigma^2 = U\tan^2\theta + V\tan\theta + W + P/\cos^2\theta$, where U, V, and W are the coefficients described by Caglioti *et al.* (*13*), and P is the Scherrer coefficient for Gaussian broadening. Preliminary refinements indicated no Gaussian broadening, so P was not refined. The Lorentzian coefficient, γ, varies as $\gamma = X/\cos\theta + Y\tan\theta + Z$, where the first term is the Lorentzian Scherrer broadening, and the second term describes strain broadening. This function (with eight parameters refined in this study) provides a better fit to asymmetric profiles and shows less correlation with the cell dimensions (*8*, *12*). The peak-profiles were truncated at 0.5% of the peak height. The background was defined by a cosine Fourier series with four terms refined simultaneously with the other profile and structural parameters. The coherent scattering lengths used were: Ca (4.70), Sr (7.02), Ba (6.00), Cu (7.72), Si (4.15), and O (5.81) fm (*14*, *15*). Intensities were corrected for the Lorentz effect. No absorption correction was applied. Low- and high-angle portions of the patterns for which only a single detector contributed were excluded, which limited the data sets to the 2θ angular range of 13.75° to 132°, or d-spacings of 5.846 to 0.7660 Å. Note that no reflections occur in the excluded region at low angles. The function minimized in the least-squares procedure was $\Sigma w_i(Y_{io} - Y_{ic})^2$, where Y_{io} and Y_{ic} are the observed and calculated intensities at each step i in the pattern. The weight w_i assigned to each step intensity is the reciprocal of the variance σ_i^2 at the ith step and was evaluated by $w_i = 1/\sigma_i^2 \approx n/Y_{io}$ where n is the number of detectors contributing to the average step intensity. The following agreement factors were calculated:

$$R_p = \Sigma|Y_{io} - Y_{ic}|\Sigma Y_{io}$$

$$R_{wp} = [\Sigma w_i(Y_{io} - Y_{ic})^2/\Sigma w_i Y_{io}^2]^{1/2}$$

$$R_{exp} = [(N - P)/\Sigma w_i Y_{io}^2]^{1/2}$$

$$\text{Goodness of fit} = \Sigma w_i(Y_{io} - Y_{ic})^2/(N - P).$$

Here N and P are the number of observations and adjustable parameters, respectively.

Starting values for the structural parameters for the refinements were obtained from the structure data of $CaCuSi_4O_{10}$ (*5*), and starting values for the peak-profile function parameters were assigned based on a previous refinement of monoclinic ZrO_2. The refinement strategy employed was as follows: 1. refine the background parameters (4) and scale factor (1), 2. include the unit cell parameters (2), 3. include positional parameters (11), 4. include anisotropic displacement parameters (26) and preferred-orientation corrections (1), and 5. include peak-profile parameters (8) allowing all adjustable parameters to vary. The preferred orientation was refined using the formulation of Dollase (*16*) and March (*17*). In all,

TABLE II

FRACTIONAL ATOMIC COORDINATES AND EQUIVALENT ISOTROPIC DISPLACEMENT PARAMETERS FOR $MCuSi_4O_{10}$ (M = Ca, Sr, Ba) IN SPACE GROUP $P4/ncc$ (ORIGIN = $8d\ \bar{1}$)[a]

	x	y	z	U_{eq} ($\times 10^3$ Å^2)[b]
Ca	¼	¾	0.0	9 (2)
Cu	¼	¼	0.0819 (1)	5 (1)
Si	0.5036 (3)	0.9267 (2)	0.1475 (1)	5 (1)
O(1)	0.4608 (2)	0.9608	¼	19 (1)
O(2)	0.7076 (2)	1.0025 (2)	0.1268 (1)	10 (1)
O(3)	0.3533 (2)	0.0068 (2)	0.0821 (1)	9 (1)
Sr	¼	¾	0.0	9 (1)
Cu	¼	¼	0.0883 (1)	6 (1)
Si	0.5088 (3)	0.9308 (3)	0.1511 (1)	6 (1)
O(1)	0.4664 (2)	0.9664	¼	20 (1)
O(2)	0.7137 (2)	1.0008 (2)	0.1311 (1)	11 (1)
O(3)	0.3667 (2)	0.0169 (2)	0.0865 (1)	12 (1)
Ba	¼	¾	0.0	8 (2)
Cu	¼	¼	0.0946 (2)	7 (1)
Si	0.5186 (4)	0.9389 (4)	0.1549 (2)	7 (1)
O(1)	0.4742 (3)	0.9742	¼	27 (2)
O(2)	0.7242 (2)	0.9988 (2)	0.1367 (1)	12 (1)
O(3)	0.3872 (2)	0.0316 (2)	0.0902 (1)	14 (1)

[a] Atom positions are M on 4b; Cu on 4c; O (1) on 8f; and Si, O(2) and O(3) on 16g.

[b] Equivalent isotropic U defined as one-third the trace of the orthogonalized U tensor.

TABLE III

SELECTED INTERATOMIC DISTANCES (Å) AND ANGLES (°) FOR GILLESPITE-TYPE COMPOUNDS

		$CaCuSi_4O_{10}$	$SrCuSi_4O_{10}$	$BaCuSi_4O_{10}$	$BaFeSi_4O_{10}$[a]
SiO_4 tetrahedra					
Si–O(1)	br[b]	1.601 (2)	1.594 (2)	1.591 (3)	1.594 (1)
Si–O(2)	br	1.619 (3)	1.626 (3)	1.620 (3)	1.620 (2)
Si–O(2)′	br	1.630 (2)	1.631 (2)	1.629 (3)	1.627 (2)
Si–O(3)	nbr	1.588 (2)	1.585 (3)	1.587 (3)	1.578 (2)
Mean		1.609	1.609	1.606	1.605
O(1)–Si–O(2)		108.2 (1)	108.3 (1)	108.9 (2)	108.5 (2)
O(1)–Si–O(2)′		109.4 (1)	109.7 (1)	108.5 (2)	109.2 (2)
O(1)–Si–O(3)		114.2 (1)	114.7 (1)	115.7 (1)	114.9 (1)
O(2)–Si–O(2)′		108.8 (1)	108.3 (1)	108.2 (2)	108.6 (2)
O(2)–Si–O(3)		112.9 (1)	111.3 (1)	110.0 (2)	110.0 (1)
O(2)–Si–O(3)		102.8 (1)	104.0 (1)	105.0 (2)	105.5 (1)
Mean		109.4	109.4	109.4	109.4
Si–O(1)–Si		176.7 (2)	177.4 (2)	176.5 (3)	177.4 (3)
Si–O(2)–Si		148.8 (2)	149.3 (2)	150.6 (2)	151.1 (2)
CuO_4 square					
Cu–O(3) ×4		1.929 (1)	1.921 (1)	1.920 (2)	1.985 (2)
O(3)–Cu–O(3)		90.000 (0)	89.987 (3)	89.920 (9)	90.
O(3)–Cu–O(3)		179.775 (1)	178.3 (2)	175.7 (2)	178.5 (2)
MO_8 distorted cube					
M–O(2) ×4		2.654 (2)	2.761 (2)	2.898 (2)	2.925 (2)
M–O(3) ×4		2.373 (1)	2.536 (1)	2.748 (2)	2.747 (2)
Mean		2.511	2.648	2.823	2.836

[a] Data from Hazen and Finger (*2*).
[b] br = bridging and nbr = nonbridging with respect to the silicate anion.

53 parameters were refined, and the least-squares refinements continued until the sum of the square errors, i.e., (parameter shifts/esd)^2, was less than 1%. The largest element in each of the correlation matrices between structural parameters was less than 0.5.

Structure Descriptions

The MCuSi$_4$O$_{10}$ (M = Ca, Sr, Ba) compounds are isostructural with the room-pressure polymorph of gillespite. The structure has six atoms in the asymmetric unit, Z = 4, and was refined using the 2nd setting of space group $P4/ncc$ (No. 130). The gillespite structure contains an unbranched single silicate layer, which can be viewed as a tesselation of corner-linked Si_4O_{10} rings (Fig. 1). The Cu in MCuSi$_4$O$_{10}$ is in square-planar coordination with the nonbridging oxygen, e.g., O(3), of the corrugations of the silicate layer. The alkaline-earth atom, in distorted cubic coordination, joins together adjacent $[CuSi_4O_{10}]^{2-}$ slabs. A summary of the refined structural parameters and agreement indices is given in Table I. The final posi-

TABLE IV

ANISOTROPIC DISPLACEMENT PARAMETERS ($\times 10^3$ Å^2) FOR MCuSi$_4$O$_{10}$ (M = Ca, Sr, Ba).

	U_{11}	U_{22}	U_{33}	U_{12}	U_{13}	U_{23}
Ca	3 (1)	3	23 (3)	0	0	0
Cu	5.5 (1)	5.5	6 (1)	0	0	0
Si	4 (1)	5 (1)	6 (1)	−0.2 (9)	−1 (1)	0.2 (9)
O(1)	28 (1)	28	1 (1)	−4 (1)	4.4 (7)	−4.4
O(2)	0.2 (8)	12.7 (9)	17 (1)	−1.9 (6)	1.6 (7)	4.3 (9)
O(3)	5.9 (8)	5.8 (9)	15 (1)	3.1 (6)	−4.0 (8)	0 (1)
Sr	7 (1)	7	11 (2)	0	0	0
Cu	4.5 (9)	4.5	10 (1)	0	0	0
Si	3 (1)	4 (1)	12 (1)	0 (1)	3 (1)	0 (1)
O(1)	27 (1)	27	6 (1)	−4 (1)	11 (1)	−11
O(2)	2.5 (9)	13 (1)	17 (1)	−2.9 (6)	1.1 (8)	5.4 (9)
O(3)	7.8 (9)	4.3 (9)	25 (1)	2.3 (6)	−8 (1)	−3 (1)
Ba	10 (1)	10	5 (2)	0	0	0
Cu	5 (1)	5	10 (2)	0	0	0
Si	6(1)	8 (1)	8 (2)	0 (1)	2 (1)	1 (1)
O(1)	36 (1)	36	10 (2)	−7 (1)	13 (1)	−13
O(2)	0 (1)	18 (1)	18 (1)	−2.2 (8)	−0.7 (9)	8 (1)
O(3)	12 (1)	5 (1)	26 (1)	5.9 (9)	−12. (1)	−3 (1)

tional parameters and equivalent isotropic displacement parameters are given in Table II. Selected bond lengths and angles are given in Table III. The refined anisotropic displacement parameters are given in Table IV.[1] The corresponding observed, calculated and difference neutron powder diffraction profiles are presented in Fig. 2.

As heavier alkaline-earth ions substitute in MCuSi$_4$O$_{10}$, the increasing length (and decreasing bond strength) of the M–O bonds systematically increases the cell dimensions and shortens the Cu–O bond length. Because of the inflexibility of the silicate anion, the expansion of the cell dimensions is anisotropic, 1.9% for a and 6.5% for c. Small, systematic bond length and angle variations within the silicate anion as a function of increasing size of the alkaline-earth ion are not apparent for the precision of the atomic positions determined. However, for the silicate anion, the expected Si–O_{br} bond length versus Si–O_{br}–Si bond angle relationship is observed (Table III) [i.e., the longer mean Si–O_{br} bonds subtend the wider Si–O_{br}–Si angle (*18, 19*)].

The equivalent isotropic displacement parameter of O(1) in each of the compounds is unusually large (Table II), which is typical of the bridging oxygen in nearly straight Si–O–Si bonds (*6*). O(1) joins adjacent four-membered rings of tetrahedra (Fig. 2). The anisotropic model (Table IV) confirms that the maximum vibration direction of O(1) is perpendicular to the Si–O–Si bond, which Hazen and Finger (*2*) also observed for gillespite. This suggests that the large vibration amplitude of O(1) reflects some slight positional disorder.

Discussion

The Cu–O bond length in BaCuSi$_4$O$_{10}$ is smaller than the Fe–O bond length in gillespite (BaFeSi$_4$O$_{10}$). Because the CuO_4 (FeO_4) square is oriented parallel to (001), the primary effect of substituting Cu for Fe is to

[1] The list of step-scan diffraction data and refined anisotropic displacement parameters have been deposited with the British Library Document Supply Centre as Supplementary Publication No. SUP 99999 (8 pp.). Copies may be obtained through The Technical Editor, International Union of Crystallography, 5 Abbey Square, Chest CH1 2HU, England.

FIG. 2. Observed, calculated, and difference neutron powder diffraction profiles for MCuSi$_4$O$_{10}$, (a) M = Ca, (b) M = Sr, and (c) M = Ba. The observed data are indicated by dots, and the calculated profile is the continuous solid line in the same field. The short vertical lines below the profiles mark the positions of all possible Bragg reflections, and the bottom curve is the difference between the observed and calculated intensity (plotted using the same vertical scale as the observed and calculated profiles).

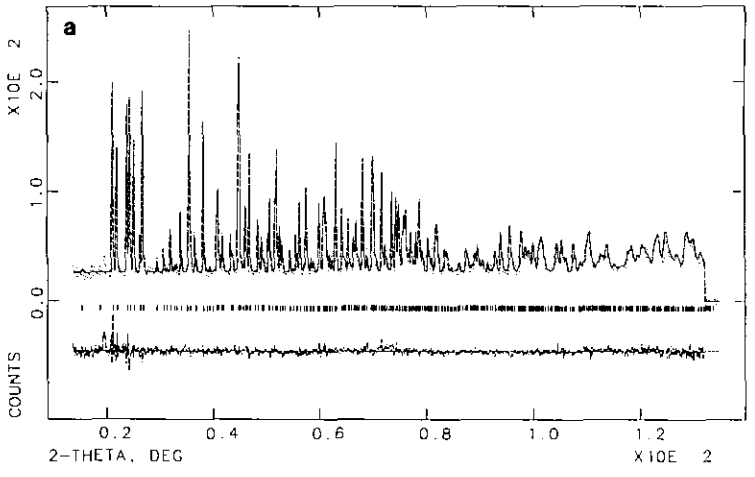
a
X10E 2
2.0
1.0
0.0
COUNTS
0.2
0.4
0.6
0.8
1.0
1.2
2-THETA, DEG
X10E 2

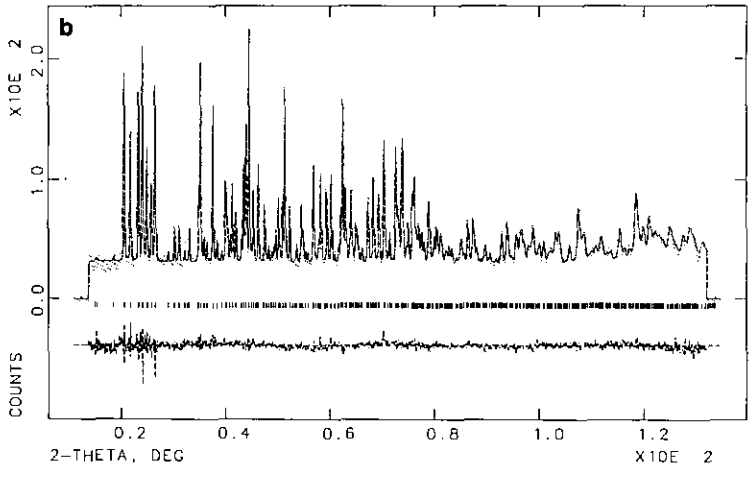
b
X10E 2
2.0
1.0
0.0
COUNTS
0.2
0.4
0.6
0.8
1.0
1.2
2-THETA, DEG
X10E 2

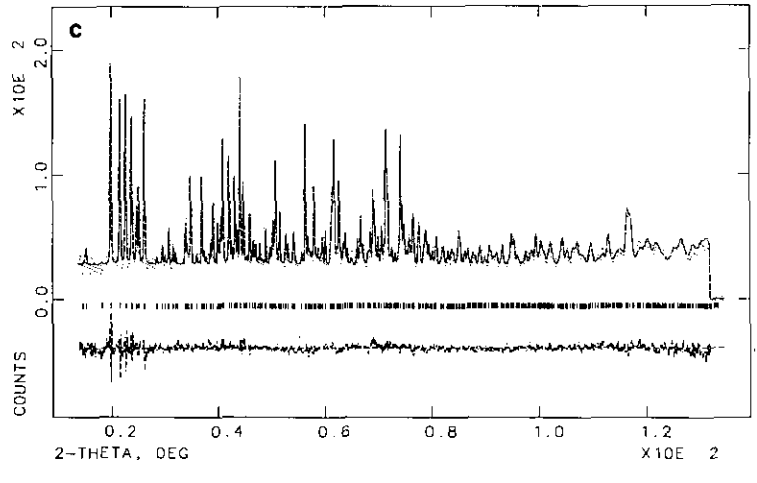
c
X10E 2
2.0
1.0
0.0
COUNTS
0.2
0.4
0.6
0.8
1.0
1.2
2-THETA, DEG
X10E 2

shorten the a cell dimension. Additionally, the stronger Cu–O bond slightly diminishes the electron density available from O(3), also bonded to Ba, thereby lengthening the Ba–O(3) bonds and increasing the c cell dimension slightly.

The MCuSi$_4$O$_{10}$ (M = Ca, Sr, Ba) compounds may exhibit high-pressure phase transitions like the gillespite I → II transition. The Ca and Sr analogs have reduced molar volumes, as compared with the Ba analog, which seemingly might stabilize the high-pressure polymorph at room-pressure; however, we see no evidence for this. If the gillespite I → II type of polymorphism does occur for the alkaline-earth copper analogs, the transitions may occur at much lower pressures. A determining factor is the difference in energy between tetrahedral distortions of the square-planar site (containing copper versus iron) which occurs for the transformation.

The question arises as to whether or not these structures intercalate oxygen, thereby increasing the formal valence of Cu to a value somewhat greater than two; and is the reversible color change observed upon annealing in either air or oxygen a manifestation of oxygen intercalation by changing the crystal field of the Cu site? Geometrically, the structure can accommodate an additional oxygen site at ($\frac{1}{4}$, $\frac{1}{4}$, z), which changes the oxygen coordination about the Cu site from a square plane to a square pyramid. Depending upon the exact value of the z coordinate, the pyramidal Cu–O bond could be shorter or longer than the equatorial Cu–O bonds. The resulting range of O···O separations is reasonable. However, an oxygen atom positioned at this site would be grossly underbonded, because only a single Cu–O bond and four very long (>3.5 Å) M–O bonds would be formed. In the extreme, if this site were half occupied, the formal Cu valence would be +3 and the ideal weight losses upon removal of the extra oxygen would be 2.1, 1.8, and 1.6 wt% for the Ca, Sr, and Ba analogs, respectively. Actually, the oxygen content of this site would probably be much less, and a local distortion of the alkaline-earth layer could improve the M–O bond strength. Thermogravimetric analysis curves of all three compounds heated to 1000°C, however, indicated no weight change in flowing oxygen and decomposition (by reducing the Cu) above 850°C in flowing nitrogen. Therefore, we conclude that these compounds do not intercalate oxygen under room-pressure conditions, and the reversible color change observed on heating in air indicates the onset of decomposition.

The square-planar geometry of the two-dimensionally infinite CuO_2 layer, characteristic of the large family of high-T_c superconducting cuprates, can be envisioned to articulate to the $CuSi_4O_{10}$ slab typical of the gillespite structure in several ways. The chemically bonded points of attachment would be the square-planar Cu sites in the silicate anion. The strain from the lattice mismatch would be reasonably small, 3–5%, as compared with the range of lattice mismatch strains of 1–8% for most of the typical perovskite-type substrates used for the growth of epitaxial $YBa_2Cu_3O_{7-d}$ thin-films. The most common unbranched single silicate anion is the hexagonal zweier layer typical of the mica group of structures. If a novel layer cuprate with silicate layers is to be realized, it would most likely incorporate one of the less common tetragonal sheet geometries like that characteristic of gillespite.

Acknowledgment

This research was supported by the Division of Materials Sciences, U.S. Department of Energy, under Contract DE-AC05-84OR21400 with Martin Marietta Energy Systems.

References

1. A. Pabst, *Am. Mineral.* **28,** 372 (1943).
2. R. M. Hazen and L. W. Finger, *Am. Mineral.* **68,** 595 (1983).

3. R. M. HAZEN AND C. W. BURNHAM, *Am. Mineral.* **59,** 1166 (1974).
4. R. M. HAZEN AND C. W. BURNHAM, *Am. Mineral.* **60,** 937 (1975).
5. A. PABST, *Acta Cryst.* **12,** 733 (1959).
6. F. LIEBAU, "Structural Chemistry of Silicates," p. 24, Springer-Verlag, New York (1985).
7. R. M. HAZEN, *Am. Mineral.* **62,** 528 (1977).
8. A. C. LARSON AND R. B. VON DREELE, "GSAS—General Structure Analysis System," Rept. LA-UR-86-748, Los Alamos National Laboratory, Los Alamos, NM 87545, (1990).
9. H. M. RIETVELD, *J. Appl. Crystallogr.* **2,** 65 (1969).
10. P. THOMPSON, D. E. COX, AND J. B. HASTINGS, *J. Appl. Crystallogr. 20,* 79 (1987).
11. C. J. HOWARD, *J. Appl. Crystallogr.* **15,** 615 (1982).
12. R. B. VON DREELE, *in* "Modern Powder Diffraction" (D. L. Bish and J. E. Post, Eds.), p. 333, The Mineralogical Society of America, Washington, DC (1989).
13. G. CAGLIOTI, A. PAOLETTI, AND F. P. RICCI, *Nucl. Instrum.* **3,** 223 (1958).
14. V. F. SEARS, *in* "Methods of Experimental Physics, Vol 23, Part A" (K. Skold and D. L. Price, Eds.), p. 521, Academic Press, Orlando (1986).
15. S. RAMAN, S. KAHANE, R. M. MOON, J. A. FERNANDEZ-BACA, J. L. ZARESTKY, J. E. LYNN, AND J. W. RICHARDSON, JR., *Phys. Review* C **39,** 1297 (1989).
16. W. A. DOLLASE, *J. Appl. Crystallogr.* **19,** 267 (1986).
17. A. MARCH, *Z. Kristallogr.* **81,** 285 (1932).
18. R. J. HILL AND G. V. GIBBS, *Acta Crystallogr. Sect. B* **35,** 25 (1979).
19. G. V. GIBBS, *Am. Mineral.* **67,** 421 (1982).
20. R. X. FISCHER, *J. Appl. Crystallogr.* **18,** 258 (1985).